Local Adaption Capabilities of Momentum Source Surrogate Propeller Models for Propeller-Aircraft Coupled Simulations

Joseph Carroll, *Member, IAENG* and David Marcum

Abstract—Many Miniature Aerial Vehicles (MAV) are driven by small scale, fixed blade propellers which can have significant impact on MAV aerodynamics. In the design and analysis process for MAVs, numerous computational fluid dynamic (CFD) simulations of the coupled aircraft and propeller are often conducted which require a time averaged, steady-state approximation of the propeller for computational efficiency. Most steady state propeller models apply an actuator disk of momentum sources to model the thrust and swirl imparted to the flowfield by a propeller. The majority of these momentum source models are based on blade element theory. Blade element theory discretizes the blade into airfoil sections and assumes them to behave as two-dimensional (2D) airfoils. Blade element theory neglects 3D flow effects that can greatly affect propeller performance limiting its accuracy and range of application.

In this paper, surrogate models for the time averaged thrust and swirl produced by each blade element are trained from a database of time-accurate, high-fidelity 3D CFD propeller simulations. Since the surrogate models are trained from these high-fidelity CFD simulations, various 3D effects on propellers are inherently accounted for such as tip loss, hub loss, post stall effect, and element interaction. These surrogate models are functions of local flow properties at the blade elements and are embedded into 3D CFD simulations as locally adaptive momentum source terms. Results of the thrust profiles for the steady-state surrogate propeller model are compared to the time-dependent, high-fidelity 3D CFD propeller simulations coupled to an aircraft. This surrogate propeller model which is dependent on local flowfield properties simulates the time-averaged flowfield produced by the propeller and captures the 3D effects and accuracy of time-dependent 3D CFD propeller blade simulations but at a much lower cost.

Index Terms—Surrogate, Propeller, blade element, computational fluid dynamics.

I. INTRODUCTION

MINIATURE Aerial Vehicles (MAV) are becoming increasingly popular in the military and domestic sectors. Many of these MAVs use small scale, fixed blade propellers for propulsion. Computational Fluid Dynamic (CFD) analysis is heavily used in the design and analysis process for these aircraft. Hundreds of CFD simulations are often conducted to determine the aerodynamic coefficients of the aircraft. Depending on the mounting configuration and sizing of the propeller, the propeller-aircraft interaction can be strongly coupled thus the propeller and aircraft must be simulated together. In many instances, the aerodynamic performance of the aircraft is significantly affected by the wake of the propeller and thus an accurate model of the flow produced by the propeller is needed.

The CFD simulation of a propeller can be performed in various ways ranging in levels of complexity. The most detailed and accurate method is to use high-fidelity 3D CFD of viscous, compressible flow to conduct a time-dependent simulation in which the propeller is rotated relative to the aircraft. For compactness, this method will be referred to in this paper as Full CFD. Full CFD propeller-aircraft coupled simulations give a highly detailed, time-accurate flowfield solution which comes at a great computational expense. Full CFD is used when a very detailed analysis of propeller flow is needed as it can capture complicated 3D flows which can significantly affect propeller performance. However, the high cost often makes this detailed and accurate method of modeling infeasible when numerous simulations are needed as is the case in determining the aerodynamic coefficients for an aircraft.

A steady-state, computationally efficient method of simulating a propeller is to view the propeller in a time-averaged sense as a source of momentum imparted to the flow. The time averaged thrust and swirl produced by a propeller is implemented into 3D CFD by embedding momentum source terms in the propeller region of the mesh. These momentum source terms are based on simplified propeller theories such as blade element theory. Blade element theory momentum source term models are well documented in literature [1]–[3]. However, these simplified theories fail to capture many of the complex 3D flow characteristics which can affect propeller performance, limiting their accuracy and range of applicability. A need exists for a low cost, steady-state propeller model which captures the accuracy of Full CFD but is applied at the momentum source level of detail.

A surrogate modeling approach first developed by Carroll's paper [4] offers a solution. Blade element theory sacrifices accuracy in determining the magnitude of the momentum source terms because it is based on 2D airfoil coefficients and thus needs many correction models. However, the model presented in this paper determines the magnitude of momentum source terms from a surrogate model which is trained with input-output data taken from a set of full 3D CFD simulations of a propeller. The input-output database for each blade element of a propeller is extracted locally at each blade element from a set of full 3D CFD propeller simulations. Training the model from full 3D CFD propeller simulations accounts for complicated 3D flow effects and in a sense has the correction models "built-in" to the training method. The momentum source terms are functions of local flow field properties and thus adapt to different

Joseph Carroll is a Ph.D. student with the Department of Mechanical Engineering at Mississippi State University funded through CAVS, Starkville, MS, 39762 USA e-mail: joecarroll28@gmail.com

David Marcum is a Professor with the Department of Mechanical Engineering at Mississippi State University, e-mail: marcum@cavs.msstate.edu

flight conditions and propeller mounting configurations. The motivation for this surrogate model comes from the need to conduct numerous CFD simulations of MAV-propeller coupled systems in which the propeller wake significantly affects the MAV aerodynamics. Therefore, the momentum source method offers the computational efficiency needed for numerous simulations, and the training method of full 3D CFD provides the high accuracy needed in predicting propeller performance.

The model development process is discussed and test cases are implemented to show the model's local adaption capabilities for aircraft coupling simulations. In the model development, an Adaptive Sequential Sampling (ASS) procedure is used to refine the design of experiment of the training simulations to reduce the overall error in the design space of the model in an optimal fashion. Polynomial regression models for the thrust and swirl produced by each blade element section are fit to the input-output data which is extracted from the full CFD training simulations. The inputs of angle of attack (α) and Reynolds number (Re) are taken locally at each blade element. These polynomial models for the momentum source terms are embedded back into a 3D CFD simulation to provide an accurate, locally adaptive, time-averaged model of the flowfield produced by the propeller. This surrogate propeller model is tested against full CFD simulations of MAV-propeller coupled scenarios.

II. 3D Effects on a Propeller

Propeller aerodynamics are quite complicated and have highly 3D flowfields. The finiteness of the blade yields complex flows around the tip. Flow circulates from the high pressure to the low pressure side causing tip vortices to be introduced into the propeller wake. These tip vortices have a detrimental effect on the thrust of a blade in the tip region; this is known as tip loss. Different blade tip geometries and propeller operating conditions result in different tip losses. In addition to tip loss, flow around the hub can also introduce vortices or flow in the spanwise direction which affects propeller performance by altering the local flow characteristics at the blade similar to a tip vortex.

The rotation of the propeller causes significant centrifugal and coriolis forces on the blade and thus on the fluid particles close to the blade surface through viscous effects. Centrifugal force causes the boundary layer to have large outward spanwise components. The coriolis force is stabilizing to the boundary layer much like a favorable pressure gradient [5]. Due to the effects of these rotational forces in the boundary layer, separation on a 3D rotating propeller blade is postponed to higher α compared to that of a nonrotational flowfield. This effect known as stall-delay is strongest near the root and decreases towards the tip proportional to increasing radial position. This delayed separation caused by 3D rotational effects has a favorable effect on propeller thrust.

III. Blade Element Theory

Blade element theory is the most common method for propeller modeling. It divides the blade into many sections in the spanwise direction which are assumed to be independent of one another. The blade elements are assumed to operate as a 2D wing in a 2D flowfield. Lift and drag characteristics of the airfoil at each blade element are used to calculate the thrust and swirl imparted to the flowfield as functions of the local α, Re, and M. The flight velocity and rotational speed of the propeller are known, however the induced velocity components are unknown. Therefore, blade element theory must be combined with another theoretical model to calculate these induced velocities. Many models exists for calculating the induced velocities such as those based on momentum theory, lifting-line theory, and a number of vortex models which describe the propeller wake in varying levels of detail.

Fundamentally, the blade element theory assumes the flow over each element to be independent and 2D in nature. However, as previously discussed, propeller aerodynamics can be highly 3D and thus not accurately predicted by 2D airfoil data. Correction models must be coupled with the blade element theory in order to compensate for errors from the simplifying 2D flow assumption and the theoretical induction models. Numerous tip loss, hub loss, and stall-delay models exist in an attempt to correct blade element models for 3D effects. However, these correction models are often empirically based and have a very limited range of applicability. Work by Carroll [6] specifically compares thrust profiles predicted by blade element codes and full CFD simulations for a typical small scale propeller used for MAVs. Significant erros are seen in thrust profiles predicted by blade element codes where 3D effects are large such as post stall operation or propellers with low aspect ratio blades. Other work supports this comparison by showing the discrepancies between thrust predictions by blade element codes compared to experimental and full CFD simulations for small scale UAV propellers with 3D effects by way of blade geometry or post stall flows [7], [8].

IV. Surrogate Modeling Procedure

A. Motivation

In a basic sense, surrogate simply means substitute, or one that takes the place of another. In the area of modeling, surrogate refers to an inexpensive approximation of a detailed, expensive computation. This efficient approximating function is developed by interpolating data from a few select cases of the expensive, high-fidelity computations. The up front cost to perform the limited number of expensive training cases and develop the surrogate may be time consuming. Nonetheless, this initial expense is cheaper than repeating the expensive computation numerous times. Surrogate modeling is applied to many disciplines, and is widely used in aerospace engineering. Performing numerous coupled propeller-aircraft full CFD simulations lends itself to a surrogate modeling of the propeller as an efficient yet accurate approximation is needed.

The surrogate-based model accounts for 3D effects such as tip loss, hub loss, and post stall effects since the training method is a 3D solution of the Navier-Stokes equations over the computational domain through the use of CFD. Contrary to blade element theory, each blade element has its own surrogate models for thrust and swirl. Therefore, no corrections models are needed to approximate the 3D effects as they are "built-in" to the training method. Applying the surrogates as steady-state models significantly reduces computation time since the problem is no longer restricted to

operate on the small time step which is needed to resolve the fast propeller rotation. The mesh size is drastically reduced as there is no need to create a mesh over the propeller blade since it is approximated by momentum sources. In addition, making the surrogates functions of local flowfield variables allows the model to adjust to different flight attitudes and aircraft couplings.

B. Propeller Geometry

The propeller chosen for simulation is a small scale propeller typically used on MAVs for low speed flight. It has a 25.4 cm diameter and two fixed blades. The term fixed blades means that the propeller blades cannot change pitch but are rigidly fixed to the hub. The blade element sections are NACA 4412 airfoils. The blade has an aspect ratio of ~ 5 based on the largest chord in the blade, and it has significant chord variation like many small scale propellers. A pictures of the propeller is shown in Figure 1. The low aspect ratio blade yields significant 3D flows which make propeller performance prediction more difficult.
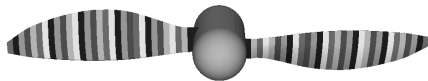

Fig. 1: Small scale propeller used in testing

C. Training Simulations

An in-house code at Mississippi State University (MSU) called CHEM [9] is used to perform the all the full CFD training simulations. CHEM is a second-order accurate, cell-centered finite volume CFD code and has been validated and applied to a wide range of problems. The unstructured grid generator AFLR3 [10], [11] is used to make all the meshes. Training simulations model the propeller in uniform flow (0 α relative to the propeller) with no other bodies in the domain. If the mounting configuration and aircraft is known and will not change throughout the application of the model, the training cases could be propeller-aircraft coupled simulations. However, an important quality of training simulations are their generality, or ability to model a wide of range of applications. Therefore, it is undesirable to restrict the training simulations to one aircraft and mounting configuration. Simulating a wide variety of isolated propeller cases covers a wide range of influential flow characteristics which will be used as surrogate model inputs. This range of inputs spanned by isolated propeller simulations includes the majority of those induced by the presence of an aircraft thus allowing these general training cases cover numerous propeller-aircraft coupling situations.

Since the flow is uniform, the propeller problem is axisymmetric about the rotational axis. This means that the flow seen by each blade is similar and steady-state in the fixed blade reference frame. Since each blade experiences rotational periodicity, only one blade needs to be modeled and the problem size can be reduced proportional to the number of blades. Therefore, periodic boundary conditions are used on the axisymmetric planes. Figure 2 shows a front view onto the rotational axis for full CFD simulations
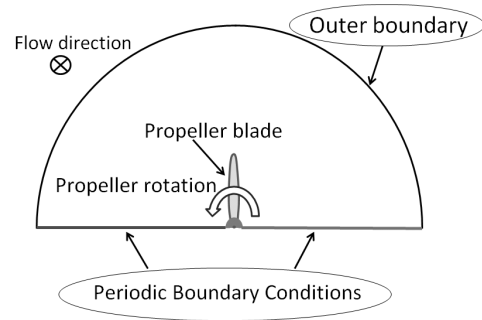

Fig. 2: Periodic domain for full CFD training simulations

setup. All training simulations are compressible, viscous and assumed to be turbulent using Menters shear stress transport (SST) turbulence model. While the Re is low ($<$ 150,000), the SST turbulence model is used to achieve settled solutions since unsteady vortex shedding occurs in regions of separation on the blade. A y+ < 5 is maintained in the first cell off the viscous surfaces for all simulations. The entire grid is rotated for time-dependent simulations in which $1°$ of rotation corresponds to 1 time-step. Each time step is refined with a number of Gauss-Seidel iterations to ensure temporal accuracy over each time-step. Simulations are run for at least 5 revolutions to achieve settled solutions without start-up effects.

D. Extracting Inputs and Outputs from Training Cases

The propeller blade is discretized into 30 blade element sections which individual surrogate models describe. To extract the outputs of axial and tangential forces (thrust and swirl) on each blade element, the surface of the blade is divided into the element sections and the CHEM code outputs output the integrated forces (viscous + inviscid) over each blade element. The radial component of force on the blade element is not included as it is negligibly small compared to the thrust and swirl values.

A propeller blade is simply a rotating wing and it is well known that α, Re, and M are main the parameters that affect the lift and drag of a wing and similarly thrust and swirl of a propeller. As with most small scale propellers, the mach number is small, < 0.25 for the case in this paper. Compressibility effects are assumed to be negligible thus only local α and Re are considered as inputs the model. It is imperative that the inputs be extracted locally at the blade element sections to allow the surrogate models to be adaptive to local changes in flowfield parameters which can be induced by different aircraft coupling configurations.

An averaging technique first developed for windmill blade aerodynamic characteristic extraction from 3D CFD simulations [12] is used to extract the local, time averaged inputs. Since the flow is uniform, a circumferential average of data from one time-step is the same as time averaging. Therefore from the last time step of a simulation, circumferential averages of velocity vectors are taken just upstream of the propeller. Figure 3 shows an annulus for a corresponding blade element over which the velocity vectors are averaged. The inputs are averaged at a constant axial position a small distance upstream (1/2 of the mean blade element chord) from the propeller plane. This upstream position for the input
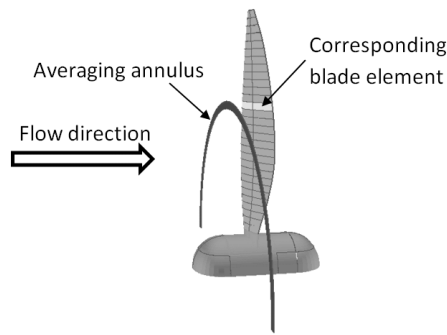
Fig. 3: Annulus region over which to take a circumferential average of the velocity vectors

extraction prevents the averaging annulus from intersecting the propeller blade allowing for a simple circumferential averaging. However, the upstream position is still close enough to the propeller so the inputs are local to each blade element and can be influenced by obstructions downstream of the propeller.

After a circumferential average of the velocity vectors, each blade element has one time-averaged local velocity vector. From this velocity vector, the local α and Re can be determined for each blade element which are used as the inputs to the surrogate model. Extracting the inputs and outputs for all the training cases gives an input-output database from which a surrogate model can be developed.

E. Optimization of the Surrogate Model

Developing a cheap surrogate model to accurately and efficiently predict the response of high-fidelity simulations over a design space depends on several factors such as the form of the surrogate model and locations of the training cases in the sampling space. An optimization process is conducted to ensure an efficient coverage of the sampling space[1] and optimal choice of the surrogate model by reducing the global error in an iterative manner [13]. The process is outlined in Figure 4. The sampling space is 2D with advance ratio (J) and rotational speed (rotations per minute - rpm) as the two variables for the simulations. Changing these global simulation parameters of J and rpm varies the local α and and Re respectively at each blade element. The bounds of the

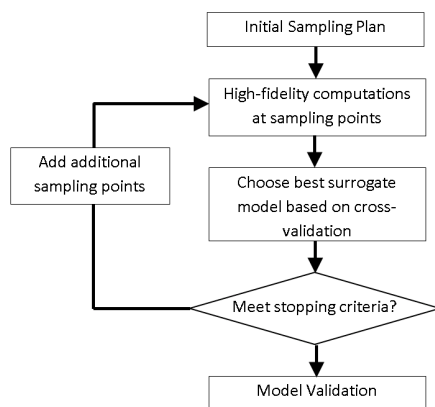[1]Thanks to Frederic Alauzet for suggesting sampling space optimization

Fig. 4: Optimization of surrogate flowchart

simulation parameters are chosen for a typical flight envelope of the propeller. J ranges from 0 to 0.6, and rpm ranges from 2000 to 6500. An Optimal Latin Hypercube (OLH) algorithm is used to create the initial sampling plan of 10 points since it has a desirable space filling property. The best surrogate model for this initial sampling plan is chosen based on leave-one-out cross-validation (LOOCV). In LOOCV, the sampling plan is divided into k subsets in which each subset leaves one sampling point out. Surrogate models are trained for each subset and then validated against the point that was left out of that particular subset. Error estimates for the propeller thrust are determined at each point by Equation 2 . Averaging the local error at each point in the sampling plan results in a global error estimation for the surrogate model. The points that make up the convex hull of the sampling plan are not included in the LOOCV error estimation process as extrapolation would occur at these points resulting in an over estimation of the error at the boundary. The mean error over all the points included in the LOOCV are assigned to the error at the convex hull points.

Polynomial regression models are used for the surrogates as the input-output relationship is relatively smooth and without spikes in the data. To determine the best form of the polynomial equation, *Mathematica* is used to create each possible polynomial form consisting of the different combinations of terms up to third order. The polynomial form is restricted to third order to prevent unrealistic oscillations and erratic behavior if extrapolation occurs. The form with the smallest global error according to LOOCV is chosen as the best surrogate model. Figure 5 shows an a polynomial response surface of the thrust output fit to the training data for a blade element at $r/R = 0.5$. Notice the smooth variation and general trend in the data which is ideally predicted by a polynomial response surface. Each blade element has its own response surface for thrust and swirl.
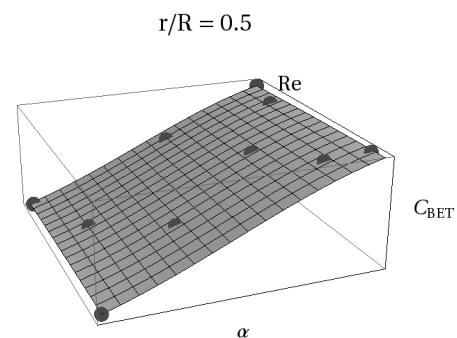
r/R = 0.5

Fig. 5: PRS of thrust for $r/R = 0.5$

A surface map of the surrogate's error over the sampling space is created using a linear radial basis function (RBF). RBF's are chosen to model the error in the sampling space as the error distribution may not be smooth, and RBF's handle data with local variations better than polynomial regressions. The locations of candidate points are determined by the OLH space filling property which considers the existing training points. The RBF of the error in teh design space is used to predict the error at each candidate point and n points with the highest error are added to the sampling plan. n is selected to be 3 for this problem, but can be adjusted based on simulation to surrogate evaluation turn around time. This optimization process of the surrogate and adaptive
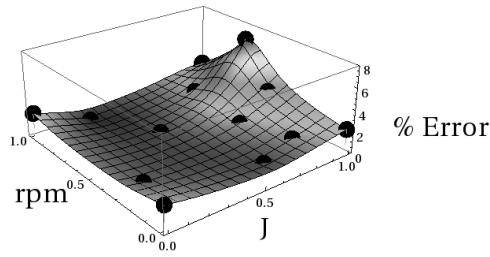
Fig. 6: Training points in design space with estimated surrogate error

Fig. 7: Grid for surrogate model

sequential sampling plan is repeated until the global error of the surrogate is sufficiently small. Only one iteration was performed. Figure 6 shows the final sampling plan of training points in the design space along with the a surface map for surrogate error estimated by LOOCV.

F. Implementing the model as momentum sources

The general form of the conservation equation of fluids for a variable ϕ is shown in Equation 1 .

$$\frac{\partial(\rho\phi)}{\partial t} + \frac{\partial}{\partial x_i}(\rho U_i \phi - \Gamma_i \phi \frac{\partial \phi}{\partial x_i}) - S_\phi = 0 \qquad (1)$$

Surrogate models for the thrust and swirl imparted to the flow are applied as momentum source terms (S_ϕ) into 3D CFD simulations. The CFD software ANSYS Fluent is chosen to implement the model since it has convenient and easy to use User Defined Functions (UDFs) for adding source terms to the flow. Source terms are applied explicitly on a per-volume basis in the propeller region of the mesh which is a cylinder approximately the same thickness and exactly the same diameter of the propeller. The mesh in the propeller region is refined to distribute the source terms over several cells in the axial direction. Distributing the source terms uniformly in the axial direction provides a smooth, stable increase in flow variables across the propeller region.

Inputs for the source terms are calculated from flow variables in cells just upstream of the propeller region. Figure 7 shows a cross section of the grid for implementing the surrogate-based source terms. This figure highlights the propeller region in which the source terms are applied and the location of the cells whose flow variables are used as inputs for the source terms. The location from which to extract the local inputs is the same as the input extraction location from the training simulations. Coupling the source terms to local flowfield variables allows the sources to adapt as the solution progresses. Adaption through the local inputs enables the surrogate propeller model to account for a wide range of aircraft couplings.

V. RESULTS AND DISCUSSION

A. Testing Method

To test the surrogate model's local adaption capabilities for various aircraft couplings, the surrogate model is implemented for propeller-aircraft coupling geometries and compared to full, unsteady CFD simulations for these same geometries and flight conditions. Recall that the training cases for the surrogate model are isolated propeller simulations in uniform flow which are intended to maintain a
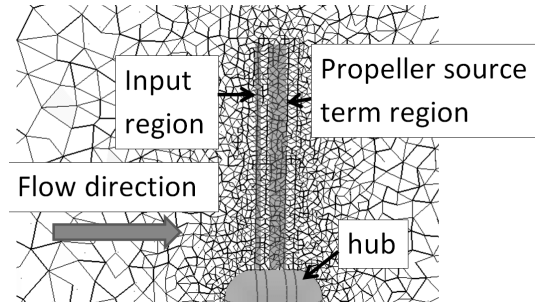
generality and not restrict the surrogate model to one aircraft coupling. The validity of using these general training cases and the local adaption capabilities are accessed by applying the surrogate momentum source to model different scenarios.

For these test cases, the flow seen by the blade is not steady state. Therefore to conduct the full CFD simulations for these test cases, the entire propeller has to be modeled and rotated relative to the aircraft in an unsteady CFD simulations performed with CHEM. To conduct a relative motion simulation, an unstructured grid with a cylindrical shape is made to encompass the propeller. The mesh on the propeller blades is similar to the training cases. Another grid is then constructed around the aircraft body, extending to the far field, which has a cylindrical hole cut out for the propeller grid. During the simulation, the grid around the aircraft is held fixed, and the propeller grid is rotated relative to the aircraft grid. The propeller grid for the relative motion cases contains 14.1 million cells alone, not including the fixed grid around the aircraft. This fine mesh is needed to resolve the complex, viscous flow around the propeller. The CHEM code is used to perform the full CFD simulation and FLUENT is used to perform the surrogate model simulations in which the momentum source terms are embedded. The two codes are comparable and both use 2nd order differencing.

The main comparison quantity is the accuracy of momentum sources. Other quantities could be compared such as the time averaged velocity in the flow field or loads on the aircraft. A paper by Zhenfeng and Yong demonstrates that if the thrust and swirl profiles in a momentum source term approach are the same as those from an unsteady, full CFD simulation, then the time averaged loads on the aircraft and velocity distribution down stream of the propeller will show good agreement [14]. Zhenfeng and Yong conduct several unsteady, RANS CFD simulations for a full scale propeller-wing coupling test case at various flight attitudes. Time averaged axial and tangential forces on the propeller are extracted from the unsteady, RANS simulations and then prescribed in a steady state momentum source CFD simulation as thrust and swirl. The time averaged loads on the wing and downstream velocity distribution in the spanwise direction match very closely between the momentum source model and the full, unsteady CFD. Zhenfeng's and Yong's work show that the time-averaged aircraft loads and flow field velocity distribution will have good agreement to a momentum source approach if the thrust and swirl profiles are correct. Therefore obtaining correct thrust and swirl profiles are the main focus for comparison.

The geometries of the "aircraft" in the test cases are simplified to allow faster simulation time. For example, the

propeller hub is not actually connected to aircraft. This makes modeling simpler and does not significantly affect propeller-aircraft coupled performance. In addition, geometric features or details of the aircraft much downstream of the propeller are not modeled. The influences of streamline geometries far downstream of the propeller do not propagate upstream enough to significantly affect propeller performance. There-fore, "aircraft" bodies in these test cases are simplified geometries chosen to induce flows which could significantly alter propeller performance.

B. Quantifying Surrogate Error

The quantity used for comparison between the blade element model and full CFD is the accuracy of the radial distribution of thrust along the blade, referred to as the thrust profile for short. Accuracy of thrust profile rather than a single integrated thrust quantity is compared because the shape of the thrust profile dictates the propeller slipstream or wake of the propeller.

Figure 8 helps visualize how the error in thrust profile is quantified. The local error is the difference in the correct and approximate thrust profile at each blade element, which is represented by the black lines in Figure 8. The approximate thrust profile in Figure 8 is a linear distribution which is just used as an example approximation in this plot. The correct thrust profile is more realistic of what one would actually see on a propeller. The average of these local errors are normalized by the mean value (represented by the horizontal line) of the correct thrust profile. The equation for this Root Mean Square Error ($RMSE$) is shown in Equation 2. f represents the full CFD (or correct) solution, $\hat{f}$ represents the blade element (or approximate) solution, and N is the number of blade elements.

$$ RMSE = \frac{1}{Mean[f]} \frac{1}{N} \sum_{i=1}^{N} \sqrt{(f_i - \hat{f}_i)^2} \qquad (2) $$

The thrust profiles are plotted in the form of C_{Thrust}/m where C_{Thrust} is defined in Equation (3). The freestream density is defined as ρ, propeller diameter is D, and n is the propeller rotational speed in $rotations/second$. Since the values used for non-dimensionalizing are global parameters and not local to each blade element, the C_{Thrust}/m plots are the same shape and simply a "scaled" scaled version of the dimensional form $Thrust/m$. Therefore thrust profile plots of C_{Thrust}/m make it easy to see the thrust distribution on the blade despite the blade geometry.

$$ C_{Thrust} = \frac{Thrust}{\rho n^2 D^4} \qquad (3) $$
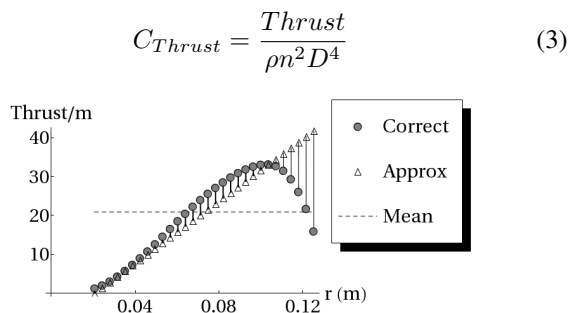

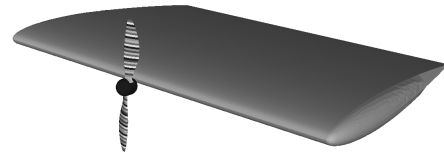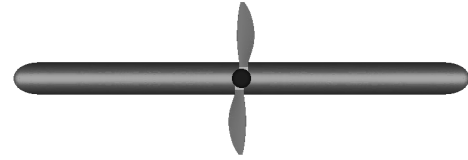Fig. 8: Plot demonstrating error calculation of thrust profile

Fig. 9: Pizza Box test case

(a) Vertical position

(b) Horizontal position

Fig. 10: Propeller positions for comparing results

C. Pizza Box

Simulations of the surrogate model are compared to a full CFD simulation for the small scale propeller coupled to a MAV with a square shaped wing that resembles a pizza box. Therefore, this test case will be referred Pizza Box. A tractor type configuration is chosen in which the propeller is mounted very close to the leading edge of the MAV. The close coupling ensures a strong two-way interaction between the propeller and MAV. Figure 9 shows a picture of the test case. The propeller operates at 0 angle of attack, a high advance ratio of 0.47, and a rpm of 6200. The advance ratio and rpm used for the test cases are different than those used for the training simulations.

The radial distribution of thrust and swirl along the blade is compared between simulations when the propeller is in two positions as shown in Figure 10. These are referred to as thrust and swirl profiles for short. Figure 11 shows the comparison of thrust and swirl between the surrogate model and full CFD for both the horizontal and vertical propeller positions. In addition, Figure 12 shows a picture of the velocity contours over a cross section from surrogate model simulation to see how the source terms impact the flow field.

The surrogate model predicts the thrust and swirl in both propeller positions with near perfect agreement to full CFD. Notice the accuracy of the surrogate model compared to full CFD in the tip and hub regions. This demonstrates the capability of the model to accurately account for the complicated 3D effects. The average error in thrust between both positions is 2.6% as calculated by Equation 2 and is a significant improvement from the error associated with the blade element theory for an isolated propeller at this flight condition. This low error is not a surprise as the predicted error for the surrogate is also low for the majority of the design space.

In the horizontal position, the thrust is higher because

(a) Thrust profile comparison for Pizza Box
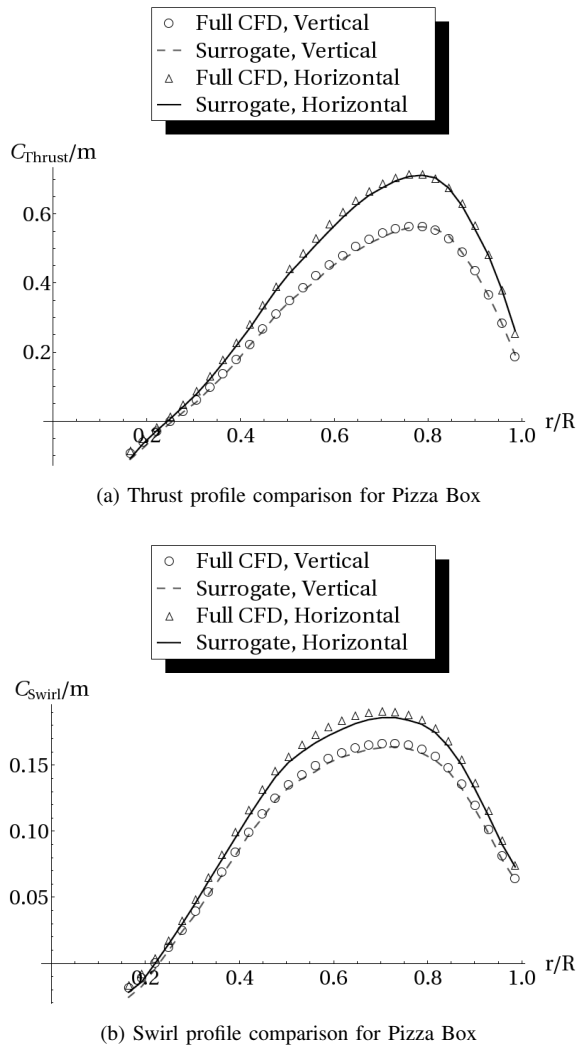

(b) Swirl profile comparison for Pizza Box

Fig. 11: Thrust and swirl profile comparison for horizontal and vertical propeller positions on Pizza Box

the propeller is sweeping through the flowfield directly in front of the MAV. Flow in the axial direction approaching the MAV slows down causing the propeller to operate at a higher angle of attack which results in a greater thrust than the vertical position. The surrogate model accurately predicts this higher thrust in the horizontal position. This highlights the capability of the local flowfield inputs to adapt the propeller performance to mounting configurations with strong aircraft-propeller coupling. Recall that the training cases only consist of full CFD simulations with no other bodies in the flow. The wide range of α and Re spanned by the training cases for each blade element cover even the inputs induced by the MAV when the propeller is in the horizontal position. The surrogate model can accurately
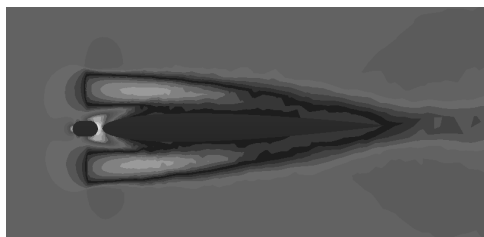

Fig. 12: Velocity contours for cross section of the MAV simulation with the surrogate model

predict aircraft coupling scenarios in which the inputs are covered by the training simulations since α and Re are the main local factors affecting the blade elements in small scale propeller performance.

In terms of computational expense, the surrogate model is much cheaper and efficient than full CFD. Table I compares several factors affecting the computational effeciency for the MAV simulations. While computational expense is saved in many ways through this surrogate model, the greatest benefit results in transferring from time-accurate to steady-state simulations. The large difference in mesh size is due to the fine body-fitted mesh around the propeller for full CFD. The computational mesh for the Pizza Box full CFD simulation is made in two parts. A mesh surrounding the propeller is rotated inside another mesh which surrounds the MAV and extends to the farfield. The mesh of the around propeller which is rotated accounts for about 90% of the total full CFD mesh size. Overall, a large reduction in computational expense without compromising accuracy is seen in this surrogate model for the Pizza Box simulation.

TABLE I: Computational Cost Factors

Factor	Full CFD	Surrogate
Mesh Size	15e6	1.5e6
Iterations for convergence	10,800	225
Problem type	Unsteady	Steady-State

D. Blunt Nose

The axisymmetric down stream obstruction test case shown in Figure 13 and nick named "Blunt Nose" is chosen to induce a flow field with significant radial velocity components much different than that of the training cases. The body is half the diameter of the propeller. While this "aircraft" or blunt nose is not realistic to something that would fly, the large diameter of the body relative to the propeller is chosen to significantly affect propeller performance to challenge the local adaption capabilities of the model. In addition, this test case intends to investigate how the surrogate model trained with only isolated propeller simulations performs when applied to a case with significant radial flow different than the training simulations.

A high $J = 0.47$ test point is selected for analysis as high advance ratios have the most significant fuselage interference or propeller-aircraft interaction. Figure 14 shows the thrust profile comparison between the surrogate model and the full CFD simulation along with the full CFD result for an isolated propeller case run at the same flight condition. This isolated
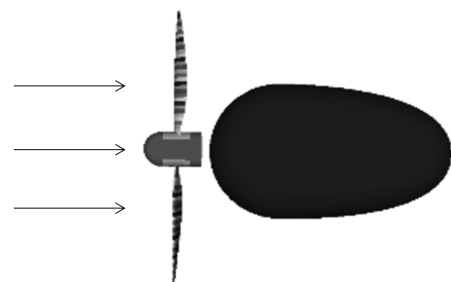

Fig. 13: Blunt Nose test case geometry

propeller thrust profile is included to show how much the presence of the blunt nose changes the performance of the propeller.
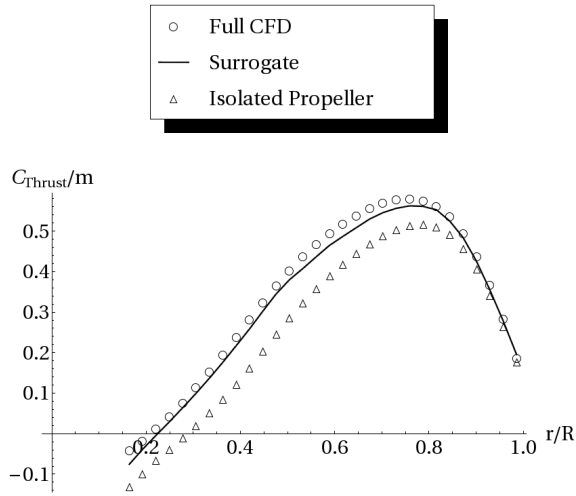

Fig. 14: Thrust Profile comparison for Blunt Puller test case

Figure 14 shows a good agreement in thrust profile between the surrogate model and full CFD with $RMSE = 5.6\%$. A strong interference effect from the blunt body on the propeller is observed by the difference in thrust profile from the isolated propeller case. The local input feature allows the surrogate model to capture this interference effect of the blunt body. While the blunt body changes the α and Re at the input plane, it also induces 3D flow that is not seen in the isolated propeller training cases. Therefore the influence of these 3D flow features induced by the blunt nose do not significantly affect propeller performance other than what the local α and Re capture.

E. P-Factor

Often times, the flight envelope for many MAVs is larger than that for conventional transport aircraft. MAVs may operate at high angles of attack causing the propeller to experience p-factor which is an asymmetric loading of the propeller. When a propeller operates at an angle of attack, the blade on the downswing side sees a greater relative wind velocity and angle of attack than on the upswing side resulting in a greater thrust on the downswing side. This results in a non-uniform loading in which the center of thrust is shifted towards the downswing side of the propeller.

The surrogate model is tested at an angle of attack to analyze its ability to predict p-factor. To isolate the effects of p-factor from fuselage interference, an isolated propeller simulation is conducted in which the propeller operates at a $30°$ angle of attack with no other bodies in the domain as shown in Figure 15. As high angle of attack flight for MAVs is typically associated with low flight speeds, a moderate advance ratio of $J = 0.27$ is selected for this p-factor test case.

Figure 16 shows the thrust profile for this moderate J test point for the p-factor case. Notice how the thrust on the bite (downswing) side is greater than the thrust on the retreating (upswing) side. This shows the non-uniform loading that occurs because the propeller operates at a high angle of attack. The surrogate model captures the different loading

on the bite and retreating sides with good accuracy in which $RMSE = 4.2\%$.

Two features of the model allow p-factor to be captured accurately, local inputs and the local non-dimensionalized output of the model. Source terms throughout the propeller region are functions of local inputs calculated from velocity vectors relative to the propeller blade. Therefore, asymmetric loading due to local changes in α at the blade elements can be captured. However, asymmetric loading in p-factor situations also results from an increased relative wind velocity at the blade on the bite side than on the retreating side. This effect is captured since the magnitude of the source terms are "unwound" from the non-dimensional PRS output using local properties relative to the propeller blade. Therefore, the p-factor contribution from greater relative wind speed on the bite side can be captured. Equation 4 and Equation 5 shows how the surrogate model outputs are non-dimensionalized. Therefore, a locally non-dimensionalized output for each blade element PRS and the use of local inputs allows p-factor to be captured sufficiently.

$$C_{BET} = \frac{F_{axial}}{\frac{1}{2}\rho V_{local}^2 A} \qquad (4)$$

$$C_{BES} = \frac{F_\theta}{\frac{1}{2}\rho V_{local}^2 A} \qquad (5)$$

$$V_{local} = \sqrt{V_{axial}^2 + V_\theta^2 + V_{radial}^2} \qquad (6)$$

$$A = (element\ length)(element\ chord) \qquad (7)$$

Another observation from the this p-factor test case is the insignificance of the unsteady effect. When a propeller operates in uniform flow at no angle of attack, the α on each blade element is constant throughout an entire revolution. However, in a p-factor situation, the angle of attack on the blade elements change in a sinusoidal manner thus making the aerodynamics unsteady. Unsteady aerodynamics of an airfoil are not only affected by α, but also $\dot{\alpha}$, and $\ddot{\alpha}$. However, the training for the surrogate model does not consider unsteady aerodynamics as the propeller operates at 0 angle of attack in the training simulations. Therefore the surrogate model prediction of p-factor ignores $\dot{\alpha}$, and $\ddot{\alpha}$ effects but still accurately predicts the p-factor. This suggest that the unsteady effects are insignificant for this case.

VI. CONCLUSION AND FUTURE WORK

In conclusion, a steady-state momentum source surrogate model is trained from a set of full CFD simulations and
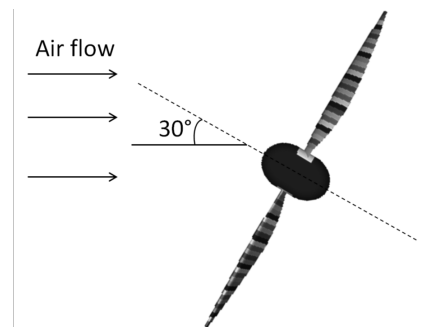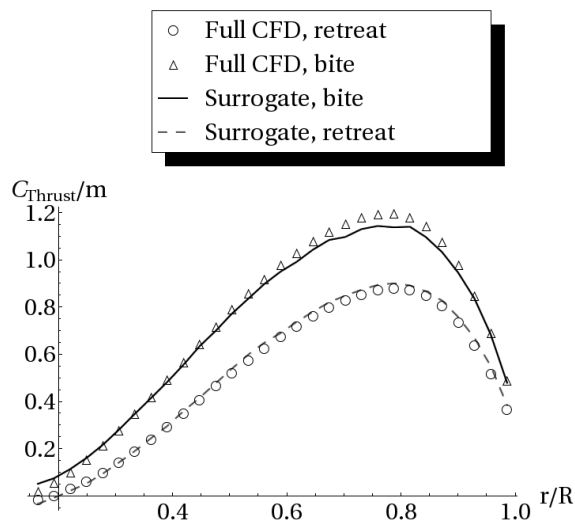

Fig. 15: P-factor test case

Fig. 16: Thrust profile comparison for p-factor test case

implemented back into 3D CFD simulations for propeller-aircraft coupled simulations. This method for propeller modeling provides an accurate and locally adaptive time-averaged model of the flow produced by the propeller. No correction models are needed for 3D effects such as tip loss and post stall performance because the nature of full CFD training cases accounts for these effects, which are known to significantly affect small scale propeller performance. The ability of the model to adapt to local flow changes induced by aircraft mounting configurations is shown for two aircraft-coupling configurations and a high angle of attack case resulting in large p-factor.

REFERENCES

[1] T. A. G. Nygaard and A. C. Dimanlig, "Application of a momentum source model to the rah-66 comanche fantail," in *American Helicopter Society 4th Decennial Specialist's Conference on Aeromechanics*, San Francisco, CA, January 2004.

[2] Rajagopalan, R. G., "A procedure for rotor performance, flowfield and interference: A perspective," in *38th Aerospace Sciences Meeting and Exhibit*, Paper No. AIAA-2000-0116, Reno, NV, January 2000.

[3] Rajagopalan, R. G., "Three dimensional analysis of a rotor in forward flight," *Journal of American Helicopter Society*, vol. 38, no. 3, pp. 14–25, 1993.

[4] Carroll, J. R. and Marcum, D. L., "Developing a Surrogate-Based Time-Averaged Momentum Source Model from 3D CFD Simulations of Small Scale Propellers," Lecture Notes in Engineering and Computer Science: Proceedings of The World Congress on Engineering 2013, U.K., 3-5 July, 2013, London, pp 1622-1627.

[5] Zondervan, G., *A Review of Propeller Modelling Techniques Based on Euler Methods*. Delft University Press, 1998.

[6] Carroll, J. R. and Marcum, D. L., "Comparison of a Blade Element Momentum Model to 3D CFD Simulations for Small Scale Propellers," in 2013 SAE AeroTech Congress and Exhibition, Paper No. 2013-01-2270, Montreal, Canada, September 2013.

[7] Kunz, P. J., "Aerodynamics and design for ultra-low reynolds number flight," PhD, Stanford University, 2003.

[8] Uhlig, D. V. and Selig, M. S., "Post stall propeller behavior at low reynolds numbers," in *4th AIAA Aerospace Sciences Meeting and Exhibit*, Paper No. 2008-407, Reno, NV, January 2008.

[9] Luke, E. and Cinnella, P., "Numerical Simulations of Mixtures of Fluids Using Upwind Algorithms," *Computers and Fluids*, Vol. 36, December 2007, pp. 1547-1566.

[10] Marcum, D. L. and Weatherill, N. P., "Unstructured Grid Generation Using Iterative Point Insertion and Local Reconnection," *AIAA Journal*, Vol. 33, No. 9, pp 1619-1625, September 1995.

[11] Marcum, D. L., "Unstructured Grid Generation Using Automatic Point Insertion and Local Reconnection," *The Handbook of Grid Generation*, edited by J.F. Thompson, B. Soni, and N.P. Weatherill, CRC Press, pp. 18-1, 1998.

[12] Johansen, J. and Sorensen, N. N., "Airfoil characteristics from 3d cfd rotor computations," *Wind Energy*, vol. 7, pp. 283–294, 2004.

[13] Mehmani, A., Zhang, J., Chowdhurry, S., and Messac, A., "A surrogate-based design optimization with adaptive sequential sampling," in *53rd AIAA/ASME/ASCE/AHS/ASC Structures, Structural Dynamics and Materials Conference*, Paper No. AIAA-2012-1527, Honolulu, HW, April 2012.

[14] Zhenfeng, X. and Yong, Y., "Time-Accurate versus Actuator Disk Simulations of Propeller Slipstream Flows," *28th International Congress of the Aeronautical Sciences*, Brisbane, Australia, 2012.